





## ARTICLE



# Transient targeting of BIM-dependent adaptive MCL1 preservation enhances tumor response to molecular therapeutics in non-small cell lung cancer

Kaixuan Shi<sup>1,7</sup>, Haijiao Lu<sup>2,7</sup>, Zhenfeng Zhang<sup>1,7</sup>, Yujie Fu<sup>3,7</sup>, Jie Wu<sup>4,7</sup>, Shichao Zhou<sup>1</sup>, Pengfei Ma<sup>3</sup>, Kaiyan Ye<sup>1</sup>, Shengzhe Zhang<sup>1</sup>, Hailei Shi<sup>4</sup>, Weiping Shi<sup>4</sup>, Mei-Chun Cai<sup>1</sup>, Xiaojing Zhao<sup>3</sup> , Zhuang Yu<sup>5</sup> , Jian Tang<sup>3</sup>  and Guanglei Zhuang<sup>1,6</sup> 

© The Author(s), under exclusive licence to ADMC Associazione Differenziamento e Morte Cellulare 2022

Despite remarkable efficacy, targeted treatments often yield a subpopulation of residual tumor cells in part due to non-genetic adaptations. Previous mechanistic understanding on the emergence of these drug-tolerant persisters (DTPs) has been limited to epigenetic and transcriptional reprogramming. Here, by comprehensively interrogating therapy-induced early dynamic protein changes in diverse oncogene-addicted non-small cell lung cancer models, we identified adaptive MCL1 increase as a new and universal mechanism to confer apoptotic evasion and DTP formation. In detail, acute MAPK signaling disruption in the presence of genotype-based tyrosine kinase inhibitors (TKIs) prompted mitochondrial accumulation of pro-apoptotic BH3-only protein BIM, which sequestered MCL1 away from MULE-mediated degradation. A small-molecule combination screen uncovered that PI3K-mTOR pathway blockade prohibited MCL1 upregulation. Biochemical and immunocytochemical evidence indicated that mTOR complex 2 (mTORC2) bound and phosphorylated MCL1, facilitating its interaction with BIM. As a result, short-term polytherapy combining antineoplastic TKIs with PI3K, mTOR or MCL1 inhibitors sufficed to prevent DTP development and promote cancer eradication. Collectively, these findings support that upfront and transient targeting of BIM-dependent, mTORC2-regulated adaptive MCL1 preservation holds enormous promise to improve the therapeutic index of molecular targeted agents.

*Cell Death & Differentiation* (2023) 30:195–207; <https://doi.org/10.1038/s41418-022-01064-2>

## INTRODUCTION

The identification of driver aberrations underlying drug sensitivity to selective kinase inhibitors has revolutionized clinical management of oncogene-addicted non-small cell lung cancer (NSCLC) over the past two decades [1]. More than 50% of lung adenocarcinomas, the major NSCLC histotype, harbor actionable molecular targets, including EGFR mutations, ALK/ROS1/RET/NTRK rearrangements, and MET exon 14 skipping variants, among others, and therefore are amenable to genotype-matched therapeutics [2]. Despite pervasive and dramatic initial efficacy, targeted treatments rarely induce complete tumor eradication, but rather retain minimal residual disease (MRD) which ultimately results in cancer relapse and represents the key obstacle to cure [3–5]. Prior studies reveal that a fraction of malignant cells acquire the ability to evade death programs and enter a drug-tolerant persister (DTP) state to serve as a reservoir for the emergence of acquired resistance [6–9], thus establishing the therapeutic potential of MRD-directed regimens. Nonetheless, the molecular

basis underpinning cell survival from lethal drug exposure remains to be fully elucidated.

At present, two non-mutually exclusive mechanisms have been uncovered to govern the formation of DTP phenotype. On one hand, the intrinsic genetic heterogeneity in a cancer cell population can allow selection and enrichment of preexisting refractory subclones through a Darwinian evolutionary process [8]. On the other hand, mounting evidence implicates non-mutational adaption of tumor cells as an alternative route toward drug tolerance [10–13]. The adaptive responses may involve a multitude of intracellular events at different layers, e.g., epigenetic dysregulation consisting of aberrant histone code [6, 14, 15], transcriptional rewiring that activates the targeted or bypass pathways [16–19], as well as the less explored alterations at protein levels. While the importance of epigenetic modifiers and transcriptional feedback loops are exemplified by a large body of recent literature, emerging roles for post-translational regulation in shaping DTP dynamics have not been comprehensively investigated.

<sup>1</sup>State Key Laboratory of Oncogenes and Related Genes, Shanghai Cancer Institute, Ren Ji Hospital, Shanghai Jiao Tong University School of Medicine, Shanghai, China.

<sup>2</sup>Department of Pulmonary Medicine, Shanghai Chest Hospital, Shanghai Jiao Tong University, Shanghai, China. <sup>3</sup>Department of Thoracic Surgery, Ren Ji Hospital, Shanghai Jiao Tong University School of Medicine, Shanghai, China. <sup>4</sup>Department of Pathology, The Affiliated Hospital of Qingdao University, Qingdao, China. <sup>5</sup>Department of Oncology, The Affiliated Hospital of Qingdao University, Qingdao, China. <sup>6</sup>Shanghai Key Laboratory of Gynecologic Oncology, Ren Ji Hospital, Shanghai Jiao Tong University School of Medicine, Shanghai, China. <sup>7</sup>These authors contributed equally: Kaixuan Shi, Haijiao Lu, Zhenfeng Zhang, Yujie Fu, Jie Wu. ✉email: zhaoxiaojing@renji.com; yuzhuang2002@163.com;

drtangjian@outlook.com; zhuanguanglei@gmail.com  
Edited by S. Kaufmann

Received: 1 December 2021 Revised: 8 September 2022 Accepted: 12 September 2022

Published online: 28 September 2022

In this study, using a range of representative lung adenocarcinoma models, we unveiled a previously unrecognized interplay between the BCL2 family proteins in promoting DTP development. Specifically, a rapid increase of MCL1 abundance was triggered by diverse targeted drugs, engendering adaptive resistance to treatment-induced programmed cell death. Mechanistically, BIM accumulation upon MAPK pathway inhibition and its sequestration of MCL1 attenuated MULE-mediated protein degradation. Of interest, the BIM-dependent MCL1 preservation was associated with MCL1 phosphorylation by mTOR complex 2 (mTORC2). Based on these findings, we proposed a rational strategy of transient polytherapy to prevent the appearance of DTP cells and potentially enhance the therapeutic index of current molecular agents.

## RESULTS

### Adaptive MCL1 upregulation in response to molecular targeted therapies

We reasoned that specific regulation at the protein level, in addition to epigenetic and transcriptional programs, might contribute to tumor cell survival from initial drug treatment. To test this hypothesis, A549 (harboring KRAS<sup>G12S</sup>), PC9 (harboring EGFR<sup>E746-A750 del</sup>) and NCI-H3122 (harboring *EML4-ALK* fusion gene) were selected and treated with genotype-matched tyrosine kinase inhibitors (TKIs), i.e., the MEK inhibitor trametinib, the EGFR inhibitor erlotinib and the ALK inhibitor crizotinib, respectively. We first considered possible roles for incomplete suppression of neoplastic signaling or inadequate induction of cell death in conferring the DTP status. As assessed by immunofluorescence staining (Fig. 1A), 48-hour TKI administration uniformly diminished ERK phosphorylation in all cells, indicating efficient inhibition of oncogenic signals. Likewise, a dramatic accumulation of BIM protein, reportedly essential for antitumor effects of targeted therapies [20, 21], was invariably observed at the single-cell level, implying potent engagement of intrinsic apoptotic machinery. However, caspase-3/7 activity was not detected within every cell, suggesting occasionally compromised capacity to stimulate subsequent activation of caspase cascade. These data pointed to a model that the mitochondrial apoptotic pathway did not properly proceed in some cases, and prompted us to perform an unbiased CRISPR (clustered regularly interspaced short palindromic repeats) screen on a focused list of key mediators. As expected, individual knockout of pro-apoptotic BIM (encoded by *BCL2L11*), cell death effector BAX, or multiple downstream factors, attenuated TKI-induced caspase-3/7 activation. On the contrary, MCL1 depletion consistently potentiated the onset of caspase-dependent apoptosis in response to small-molecule inhibitors (Fig. 1B). In the meantime, we examined dynamic changes of putative apoptogenic regulators, in particular the BCL2 family members [22], and found that MCL1 protein was notably upregulated with prolonged drug exposure (Fig. 1C). Intriguingly, elevated MCL1 gradually declined following compound withdrawal, demonstrating the reversibility of this phenomenon (Fig. 1D). Of clinical relevance, although it was not feasible to monitor MCL1 levels immediately after treatment, we noted that in a large cohort of lung adenocarcinoma with distinct genetic alterations, MCL1 exhibited prominent expression, as evidenced by positive immunohistochemical staining in 64.7% of KRAS-mutant, 62.4% of EGFR-altered and 54.9% of ALK-rearranged tumor specimens (Fig. 1E) using a validated antibody (Supplementary Fig. 1A). These observations were extended to a panel of lung cancer cell lines encompassing different oncogenic drivers and expressing various amounts of BCL2 family proteins (Supplementary Fig. 1B). MCL1 induction by relevant TKIs was confirmed in diverse models harboring EGFR, ALK, MET, HER2, KRAS or BRAF aberrations (Supplementary Fig. 1C). Taken together, we identified adaptive MCL1 upregulation as a new candidate mechanism by

which oncogene-addicted tumor cells could survive the profound antagonistic effects of molecular targeted therapies.

### Genetic or pharmacological MCL1 inhibition enhances tumor response to molecular therapeutics

To validate the essential role of MCL1 in the setting of DTP formation, MCL1 was knocked out using two different single-guide RNAs (sgRNAs) in A549, PC9 and NCI-H3122 cells. Genetic MCL1 deletion did not significantly affect cell viability at baseline, but evidently sensitized lung cancer to TKI treatment and resulted in fewer surviving DTP cells (Fig. 2A). Consistently, MCL1 loss led to a marked decrease of IC<sub>50</sub> (compound concentration causing 50% inhibition) in all three cell lines (Fig. 2B). Western blot analysis showed that 48-hour drug exposure yielded more cleaved caspase-3, PARP and GSDME in MCL1-depleted cells, demonstrating enhanced apoptosis and pyroptosis (Fig. 2C). In line with these in vitro findings, MCL1 ablation in conjunction with small-molecule inhibitors efficaciously blocked tumor growth in mouse xenograft models (Fig. 2D). To complement the genetic data, we exploited a pharmacological tool, S63845, a BH3 mimetic with exceptional selectivity and potency against MCL1 [23]. When combined with targeted agents, S63845 effectively activated both apoptotic and pyroptotic cell death, as indicated by caspase-3, PARP and GSDME cleavage (Fig. 2E), as well as cytochrome c leakage from mitochondria into cytosol (Supplementary Fig. 2A). We also performed dose matrix assays to assess the effects of drug combination using the Bliss independence model. The heatmaps for Bliss synergy scores illustrated that each TKI and S63845 synergistically reduced tumor cell viability (Fig. 2F), which was further verified by crystal violet staining (Fig. 2G) and IC<sub>50</sub> measurements (Supplementary Fig. 2B). Similar results were obtained in a spectrum of oncogene-driven cell lines treated with S63845 and corresponding targeted inhibitors (Supplementary Fig. 2C). Therefore, genetic or pharmacological MCL1 inhibition impeded DTP generation and enhanced tumor response to molecular therapeutics.

### Molecular targeted therapies induce BIM-dependent MCL1 preservation

A better understanding of molecular mechanisms controlling MCL1 upregulation in response to TKI could offer improved treatment strategies capable of unleashing the full potential of targeted therapies. To this end, we first investigated transcriptional profiles of the BCL2 family genes by RNA sequencing (RNA-seq) (Fig. 3A) and quantitative PCR (Supplementary Fig. 3A) in A549, PC9 and NCI-H3122 cells. Unlike transcripts of BIM (known as *BCL2L11*), MCL1 expression was not consistently augmented by oncogene-directed inhibitors in the three cell lines, implying that post-transcriptional mechanisms might underlie adaptive MCL1 upregulation. Given the distinctive instability of MCL1 protein, we focused on its reported E3 ubiquitin ligases including MULE and FBW7, which could poly-ubiquitylate MCL1 for proteasomal degradation [24–26]. Transient knockdown of *FBXW7* (encoding FBW7) resulted in moderately elevated MCL1 at basal levels but failed to block further gain upon targeted agents (Supplementary Fig. 3B). In contrast, no TKI-elicited MCL1 increase occurred with MULE depletion (Fig. 3B), supporting a central role for MULE in this context. As a matter of fact, MULE is a unique E3 ubiquitin ligase that contains the conserved BH3 domain [24], through which the BCL2 family members interact with each other. Interestingly, we found that MAPK, rather than PI3K, pathway inhibition positively modulated both BIM and MCL1 levels (Supplementary Fig. 3C). Therefore, we speculated that during TKI treatment, induced pro-apoptotic BH3-only proteins, such as BIM, would compete with MULE to bind MCL1 and consequently protect MCL1 from the proteolytic system. Indeed, all the three small-molecule inhibitors stimulated colocalization of MCL1 and BIM (Fig. 3C) and promoted their interaction while dissociating MCL1 from MULE (Fig. 3D). Importantly, MCL1 enrichment caused by drug incubation was markedly impaired by genetic deletion of *BCL2L11* (encoding BIM) using two different sgRNAs (Fig. 3E). As a control,

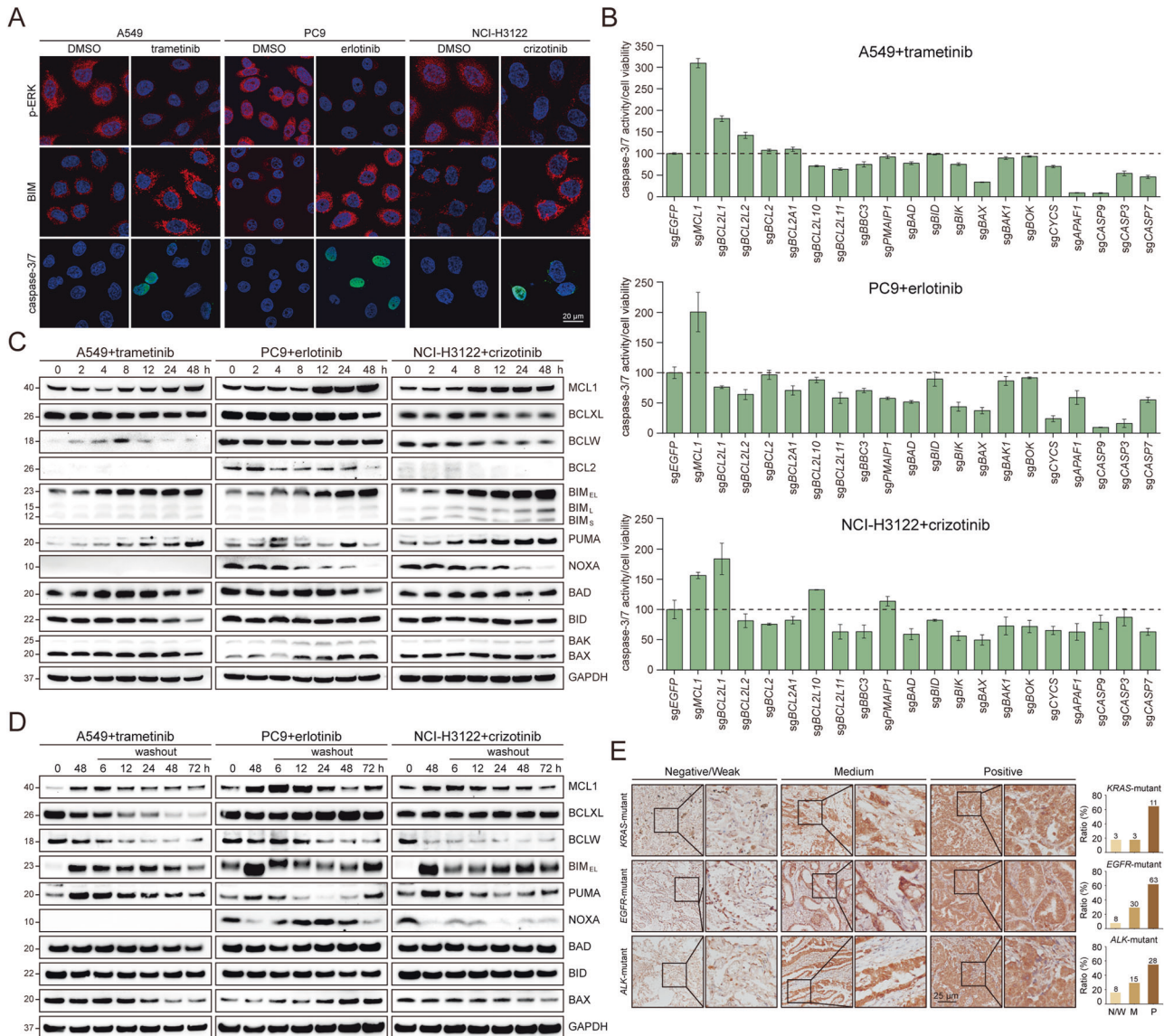


**Fig. 1 Adaptive MCL1 upregulation in response to molecular targeted therapies.** **A** Representative immunofluorescent images of phosphorylated ERK (p-ERK, T202/Y204), BIM protein and caspase-3/7 activatable nuclear dye in A549, PC9 and NCI-H3122 cells treated with DMSO or indicated inhibitors (trametinib: 1  $\mu$ M; erlotinib: 1  $\mu$ M; crizotinib: 3  $\mu$ M). Scale bar, 20  $\mu$ m. **B** A549, PC9 and NCI-H3122 cells were infected with lentiviral sgRNAs targeting selected genes in the mitochondrial apoptotic pathway, and treated with indicated inhibitors for 72 h (trametinib: 1  $\mu$ M; erlotinib: 1  $\mu$ M; crizotinib: 3  $\mu$ M). Caspase-3/7 activity and cell viability were measured by Caspase-Glo 3/7 and CellTiter-Glo assays, respectively. Results were presented as the ratio of caspase-3/7 activity/cell viability. Each column represented the mean value of three biological replicates, and error bars indicated standard deviation. **C** A549, PC9 and NCI-H3122 cells were treated with indicated inhibitors over a time course (trametinib: 1  $\mu$ M; erlotinib: 1  $\mu$ M; crizotinib: 3  $\mu$ M), and cell lysates were analyzed by immunoblotting. **D** A549, PC9 and NCI-H3122 cells were treated with indicated inhibitors for 48 hours (trametinib: 1  $\mu$ M; erlotinib: 1  $\mu$ M; crizotinib: 3  $\mu$ M), followed by drug withdrawal lasting various durations. Cell lysates were analyzed by immunoblotting. **E** Immunohistochemical staining of MCL1 in a cohort of KRAS-mutant (17 samples), EGFR-altered (101 samples) or ALK-rearranged (51 samples) lung adenocarcinoma. Representative images and quantification for negative/weak, medium or positive staining were shown.

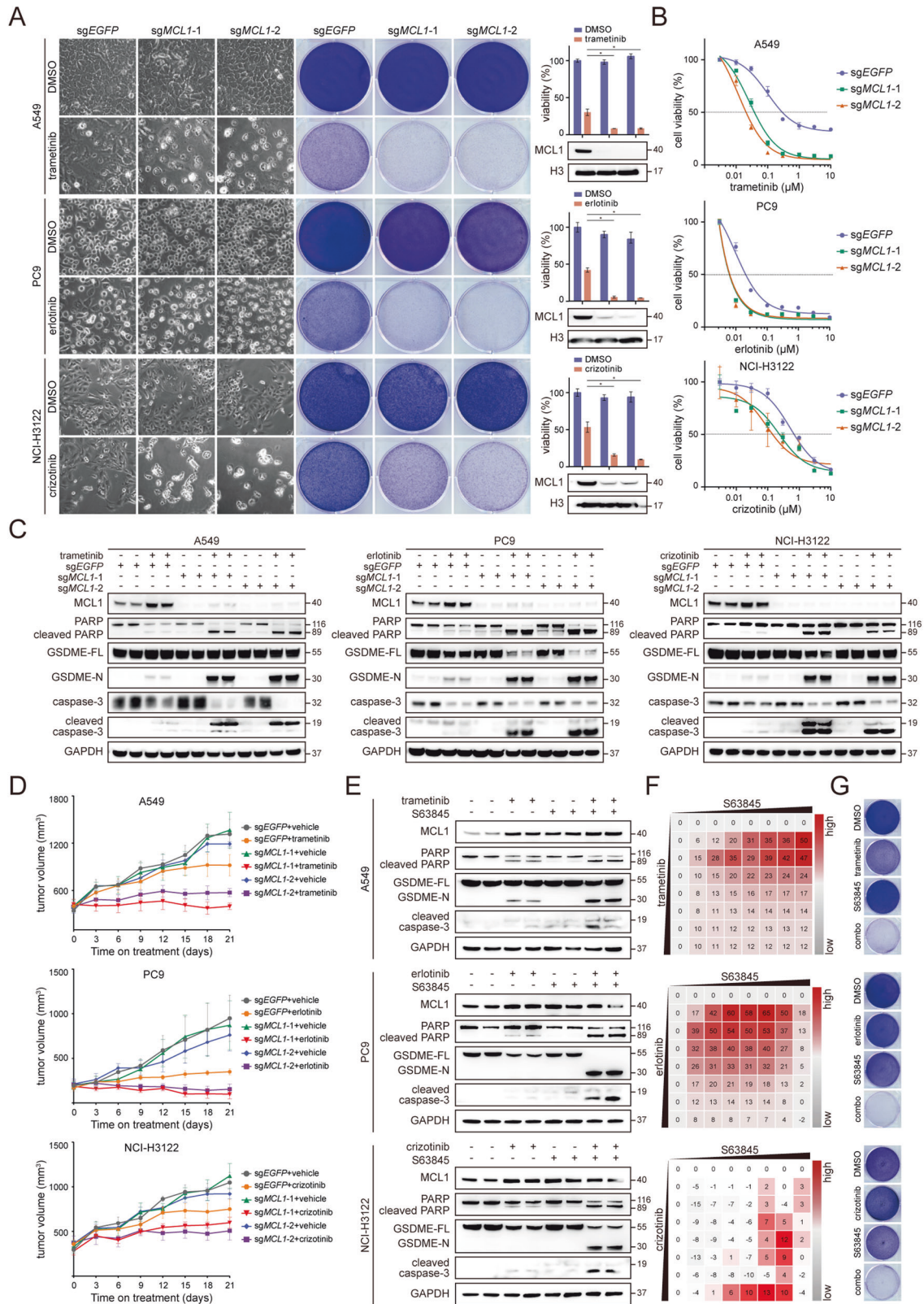
CASP3 (encoding caspase-3) or BAX knockout (Supplementary Fig. 3D) and pan-caspase inhibitor Q-VD-OPh (Supplementary Fig. 3E) did not abrogate MCL1 accumulation, obviating the requirement of caspase-executed cell death. Collectively, adaptive MCL1 upregulation was most likely due to BIM-dependent MCL1 preservation from MULE-mediated ubiquitination and degradation.

#### BIM-associated adaptive MCL1 preservation is tuned by mTORC2-mediated MCL1 phosphorylation

To further fulfill the therapeutic potential of these findings, we probed whether adaptive MCL1 increase was regulated by

actionable tumorigenic pathways by performing a combination drug screen with diverse small-molecule inhibitors (Fig. 4A). Flavopiridol, a pan-CDK inhibitor previously reported to suppress MCL1 transcription [27], almost completely ablated MCL1 expression. In addition, PI3K inhibitor GDC-0941 (Fig. 4B) and mTOR inhibitor AZD8055 (Fig. 4C) were noted to abolish MCL1 upregulation, which was subsequently validated utilizing a PI3Ka inhibitor BYL719 (Supplementary Fig. 4A) and another ATP-competitive mTOR inhibitor Torin1 (Supplementary Fig. 4B). It has been well documented that the PI3K-mTOR axis may rebound during prolonged exposure of targeted agents [10]. Hence, our





data suggested that such a feedback loop might dictate MCL1 stability in the context of oncogene inhibition. The mTOR kinase exists in two distinct complexes, termed mTORC1 and mTORC2, both downstream of the PI3K signaling [28]. The mTORC1-specific inhibitor everolimus failed to block MCL1

elevation (Supplementary Fig. 4C), implying a pivotal role of mTORC2 in MCL1 preservation. Supporting this notion, genetic inactivation of mTORC2 by knocking out its key component RICTOR mitigated adaptive MCL1 upregulation (Fig. 4D). Surprisingly, none of the canonical mTORC2 substrates, including AKT

**Fig. 2 Genetic or pharmacological MCL1 inhibition enhances tumor response to molecular therapeutics.** **A** The *MCL1* gene was knocked out in A549, PC9 and NCI-H3122 cells using the CRISPR-Cas9 system, and MCL1 protein was analyzed by immunoblotting. Drug response (trametinib: 1  $\mu$ M; erlotinib: 1  $\mu$ M; crizotinib: 3  $\mu$ M) upon *MCL1* depletion was assayed by phase-contrast microscopy or crystal violet staining, and quantified as shown in bar graphs. \* $P < 0.05$ , ANOVA followed by Tukey's post-test. **B** The *MCL1* gene was knocked out in A549, PC9 and NCI-H3122 cells using the CRISPR-Cas9 system. Cell viability in the presence of various concentrations of indicated inhibitors was measured. Genetic *MCL1* deletion did not affect cell viability at baseline, but decreased  $IC_{50}$  in all three cell lines. **C** The *MCL1* gene was knocked out in A549, PC9 and NCI-H3122 cells, followed by treatment with indicated inhibitors (trametinib: 1  $\mu$ M; erlotinib: 1  $\mu$ M; crizotinib: 3  $\mu$ M). Cell lysates were analyzed by immunoblotting. GSDME-FL, full-length GSDME; GSDME-N, GSDME N-terminal domain. **D** Tumor growth curves of MCL1-depleted A549, PC9 and NCI-H3122 cells. The xenografts were treated with vehicle control or indicated inhibitors. Each line represented the mean tumor volume and error bars indicated standard deviation (10 mice/group). **E** A549, PC9 and NCI-H3122 cells were treated with indicated inhibitors either alone (trametinib: 1  $\mu$ M; erlotinib: 1  $\mu$ M; crizotinib: 3  $\mu$ M), or in combination with MCL1 inhibitor S63845 (1  $\mu$ M). Protein markers for apoptosis and pyroptosis were analyzed by immunoblotting. **F** Heatmaps of bliss synergy scores demonstrated synergistic activities of indicated inhibitors and MCL1 inhibitor S63845 in A549, PC9 and NCI-H3122 cells. **G** A549, PC9 and NCI-H3122 cells were treated with indicated inhibitors (trametinib: 1  $\mu$ M; erlotinib: 1  $\mu$ M; crizotinib: 3  $\mu$ M) and analyzed by crystal violet staining.

(Supplementary Fig. 4D), PKC (Supplementary Fig. 4E) and SGK (Supplementary Fig. 4F), were involved in MCL1 stabilization, as analyzed by using their respective inhibitors. Therefore, we considered the possibility of direct MCL1 phosphorylation and regulation by mTORC2. Immunofluorescence staining revealed mitochondrial colocalization between MCL1 and mTOR (Supplementary Fig. 5A) or RICTOR (Supplementary Fig. 5B) following TKI treatment. Proximity ligation assay (Fig. 4E) and co-immunoprecipitation experiment (Fig. 4F) demonstrated that MCL1 indeed interacted with mTORC2 at the endogenous level. Examination of MCL1 protein sequence uncovered that the serine 64 (S64) residue was evolutionally conserved among different species and characterized by an SPP motif, similar to the phosphorylation sites (TPP) located in the turn motif (TM) of known mTORC2 substrates (Supplementary Fig. 5C). We thus performed in vitro kinase assays with immunoprecipitated mTORC2, which was found to directly phosphorylate purified MCL1 protein at S64 (Fig. 4G). Importantly, in accordance with previous studies [29], S64 phosphorylation seemed to facilitate protein binding of MCL1 and BIM (Supplementary Fig. 5D). Consistently, mTORC2 blockade with AZD8055 resulted in concerted reduction of MCL1 abundance, MCL1 S64 phosphorylation, and complex formation between MCL1 and BIM (Fig. 4H). We concluded that BIM-associated adaptive MCL1 preservation was tuned by mTORC2-mediated MCL1 phosphorylation, providing a new avenue for therapeutic intervention.

### Transient targeting of adaptive MCL1 preservation provokes tumor cell death

In light of the adaptive MCL1 upregulation, we envision that upfront polytherapy combining oncogene-targeting medicine and MCL1-disrupting agents will improve patient outcome by hindering MRD development. However, one major concern is conceivably intensified side effects associated with simultaneously applying multiple drugs in the clinical setting [30]. Rational design of short-term combinational treatment represents an attractive strategy to increase safety profile while maintaining therapeutic efficacy. As anticipated, transient combination of GDC-0941, AZD8055, or S63845 with TKI resembled continuous drug administration to eradicate residual tumor cells (Fig. 5A). At the molecular level, 48-hour inhibitor combo was sufficient to provoke tumor cell death by inducing cytochrome c release, caspase-3/7 activation (Fig. 5B), as well as caspase-3 and PARP cleavage (Fig. 5C). We also evaluated a vertical inhibition approach by co-targeting upstream oncogenic drivers and downstream anti-apoptotic proteins at suboptimal drug concentrations. Low-dose combination of TKI and compounds reducing (GDC-0941 or AZD8055) or blocking MCL1 (S63845) proved to achieve comparable performance to high-dose regimens, as indicated by cell viability assessment (Supplementary Fig. 6A), cytochrome c release and caspase-3/7 activation (Supplementary Fig. 6B), as well as caspase-3 and PARP cleavage (Supplementary

Fig. 6C). Remarkably, in vivo studies recapitulated the in vitro findings and demonstrated that the initial addition of GDC-0941, AZD8055, or S63845 to trametinib was sufficient to efficaciously inhibit A549 xenograft growth in mice (Fig. 6A), without evident loss of body weight (Supplementary Fig. 7A) or histological abnormality in heart, liver, spleen, lung and kidney (Supplementary Fig. 7B). Compared with the single-agent effects of trametinib, brief drug exposure to GDC-0941, AZD8055, or S63845 led to notably smaller subcutaneous implants (Fig. 6B), an approximately twofold reduction in tumor burden (Fig. 6C), and a dramatic increase of cell apoptosis as marked by cleaved PARP and caspase-3 (Fig. 6D). On the basis of these results, we propose that transient targeting of adaptive MCL1 preservation or low-dose vertical treatment protocols should suffice to prevent DTP formation and improve the therapeutic index of molecular targeted therapies.

### DISCUSSION

The BCL-2 family proteins are key regulators of programmed cell death by controlling mitochondrial outer membrane permeabilization [22]. Their promiscuous interplay, involving the BH3 domain of pro-apoptotic members binding to a hydrophobic groove on the anti-apoptotic counterparts, governs cellular commitment to perturbation-induced apoptosis. In the case of oncogene-directed treatment, pro-death signals, e.g., through BIM accumulation, overwhelm the pro-survival reserve such as MCL1, tipping the balance towards an apoptotic outcome. Here, we revealed that this particular interaction also preserved MCL1 from MULE-mediated degradation, which partially restored the BIM/MCL1 equilibrium and aided apoptotic evasion. Of importance, feedback PI3K-mTORC2 activation, reportedly as a result of transcriptional reprogramming [10], participated in the regulation, implying potential crosstalk between different modes of non-genetic adaptation. Based on these findings, rational targeting of adaptive MCL1 preservation following diverse molecular therapies was proposed to prevent DTP emergence and enable complete cancer cell eradication (summarized in Fig. 6E).

Although a wealthy literature has implicated MCL1 in tumor development and drug response [31–36], the adaptive MCL1 increase described in this study notably differs from previous observations in the context of anticancer treatment. For example, it was reported that MCL1 downregulation dictated chemotherapeutic efficacy [26], and MCL1 upregulation proved to confer acquired resistance to various cytotoxic agents [37–40]. More recently, MCL1 biosynthesis was shown to be augmented to support cell survival in the established DTP population [41]. In contrast, we focused on drug tolerance dynamics during initial TKI exposure, and identified therapy-elicited MCL1 elevation as a pervasive and reversible route toward the DTP phenotype. Therefore, our data provided new insights into early molecular events underlying the formation of minimal residual disease.



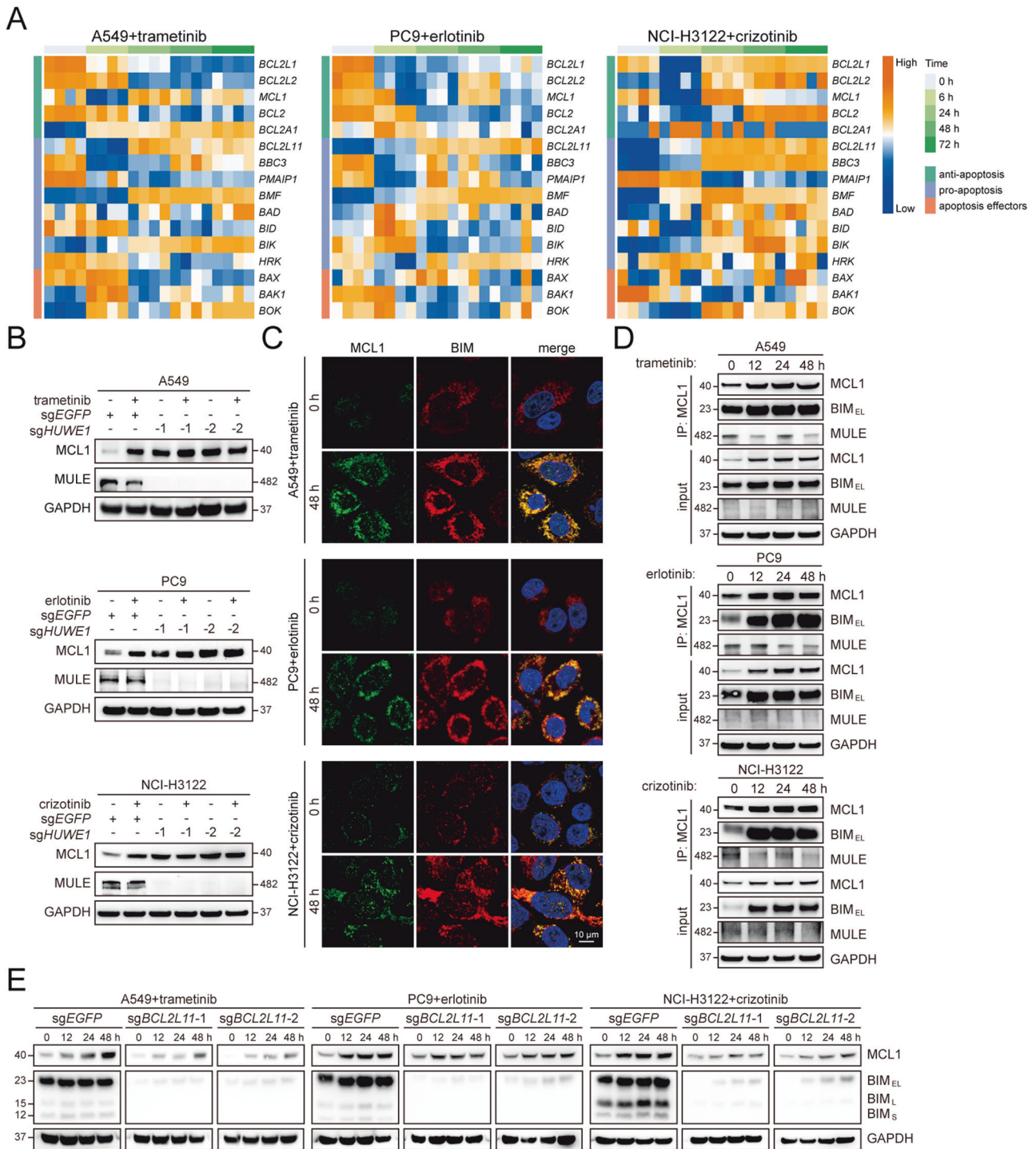
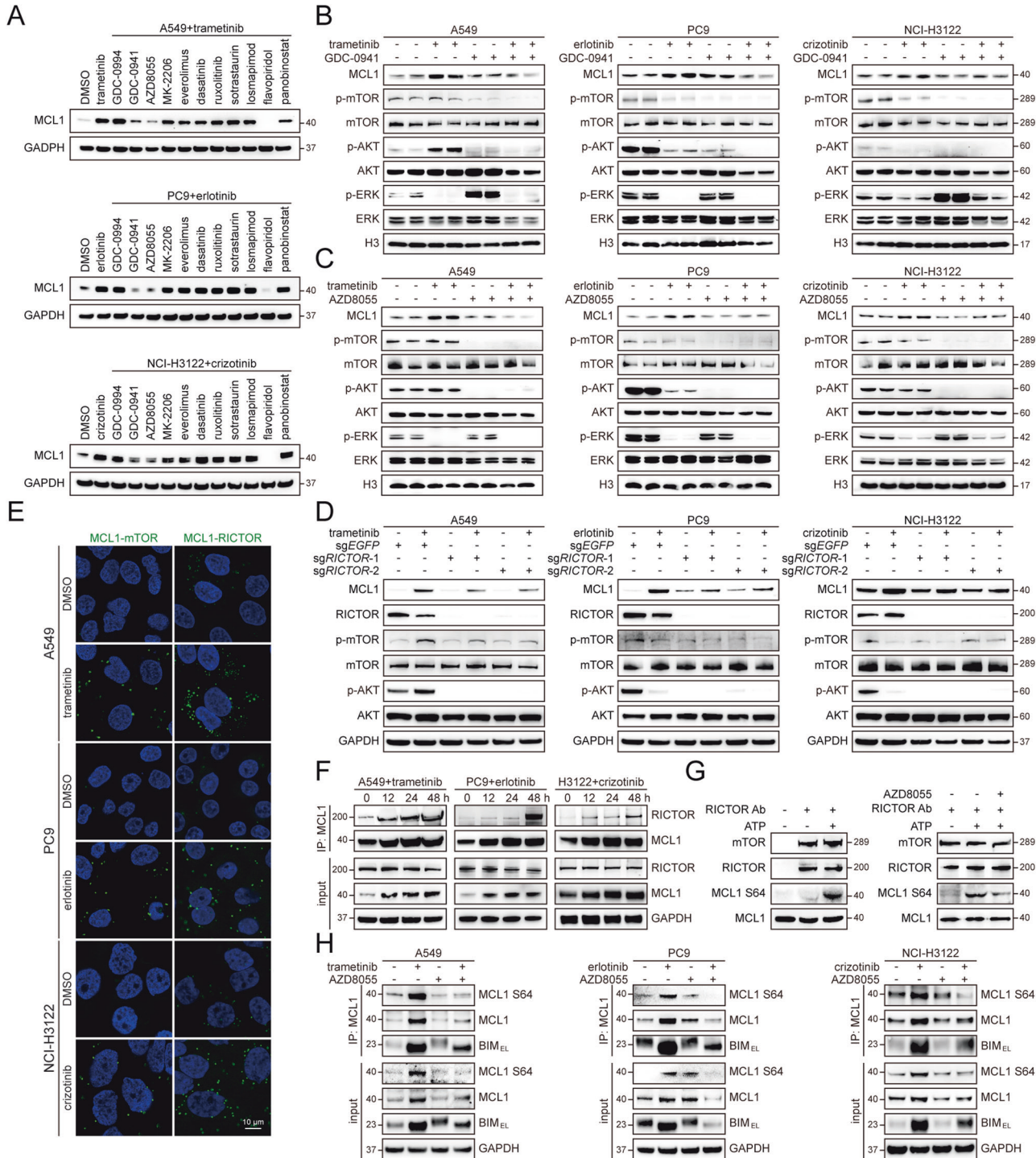


**Fig. 3 Molecular targeted therapies induce BIM-dependent MCL1 preservation.** **A** A549, PC9 and NCI-H3122 cells were treated with indicated inhibitors over a time course (trametinib: 1  $\mu$ M; erlotinib: 1  $\mu$ M; crizotinib: 3  $\mu$ M), and analyzed by RNA-seq. Heatmaps showed expression levels of the BCL2 family genes. **B** The *HUWE1* gene (encoding MULE) was knocked out in A549, PC9 and NCI-H3122 cells, followed by treatment with indicated inhibitors (trametinib: 1  $\mu$ M; erlotinib: 1  $\mu$ M; crizotinib: 3  $\mu$ M). Cell lysates were analyzed by immunoblotting. **C** Representative immunofluorescent images of MCL1 and BIM staining in A549, PC9 and NCI-H3122 cells treated with DMSO or indicated inhibitors (trametinib: 1  $\mu$ M; erlotinib: 1  $\mu$ M; crizotinib: 3  $\mu$ M). Scale bar, 10  $\mu$ m. **D** A549, PC9 and NCI-H3122 cells were treated with indicated inhibitors over a time course (trametinib: 1  $\mu$ M; erlotinib: 1  $\mu$ M; crizotinib: 3  $\mu$ M). Endogenous MCL1 protein was immunoprecipitated and probed for BIM interaction. **E** The *BCL2L11* gene (encoding BIM) was knocked out in A549, PC9 and NCI-H3122 cells, followed by treatment with indicated inhibitors (trametinib: 1  $\mu$ M; erlotinib: 1  $\mu$ M; crizotinib: 3  $\mu$ M). Cell lysates were analyzed by immunoblotting. The related blots were cropped from one membrane with the same exposure for the convenience of data presentation.



Specifically, oncogene inhibition caused a rapid induction of pro-apoptotic protein BIM, which paradoxically antagonized MCL1 function while preserved its expression, reminiscent of reciprocal protection between steady-state BIM and MCL1 from the ubiquitin-proteasome system [42, 43]. In reverse, the increased levels of MCL1 might bind and neutralize BIM and apoptotic effectors, such as BAK and BAX, rendering some tumor cells poised but refractory to robust apoptosis. Together, these results reinforce the emerging notion that relative expression and intricate competition of BCL-2 family members synchronously determine differential apoptotic response to antineoplastic therapeutics [31–33]. Along this line, we noted that the levels of

BCLXL protein were invariably high in NSCLC, arguing for its biological significance which warrants future investigations.

The relief of negative feedback loops is a prevalent phenomenon following targeted treatments, which involves transcriptional induction of upstream growth factor receptors and serves as a mechanism of adaptive resistance to administered antitumor agents [10, 11, 16]. Indeed, we observed PI3K and MAPK reactivation upon prolonged drug exposure, and further demonstrated that the rebounded PI3K-mTOR signaling contributed to BIM-dependent MCL1 preservation. Therefore, both transcriptional and post-translational adaption intersected and converged on MCL1 stabilization. Downstream of the PI3K-mTOR axis, MCL1 has



**Fig. 4 BIM-associated adaptive MCL1 preservation is tuned by mTORC2-mediated MCL1 phosphorylation.** **A** A549, PC9 and NCI-H3122 cells were treated with indicated inhibitors either alone or in combination for 48 h (crizotinib: 3  $\mu$ M; others: 1  $\mu$ M). Cell lysates were analyzed by immunoblotting. **B** A549, PC9 and NCI-H3122 cells were treated with indicated inhibitors either alone (trametinib: 1  $\mu$ M; erlotinib: 1  $\mu$ M; crizotinib: 3  $\mu$ M), or in combination with PI3K inhibitor GDC-0941 (1  $\mu$ M) for 48 h, and cell lysates were analyzed by immunoblotting. The following phosphorylation-specific antibodies were used: p-mTOR (S2481), p-AKT (S473), p-ERK (T202/Y204). **C** A549, PC9 and NCI-H3122 cells were treated with indicated inhibitors either alone (trametinib: 1  $\mu$ M; erlotinib: 1  $\mu$ M; crizotinib: 3  $\mu$ M), or in combination with mTOR inhibitor AZD8055 (1  $\mu$ M) for 48 h, and cell lysates were analyzed by immunoblotting. The following phosphorylation-specific antibodies were used: p-mTOR (S2481), p-AKT (S473), p-ERK (T202/Y204). **D** The *RICTOR* gene was knocked out in A549, PC9 and NCI-H3122 cells, followed by treatment with indicated inhibitors. Cell lysates were analyzed by immunoblotting. The following phosphorylation-specific antibodies were used: p-mTOR (S2481), p-AKT (S473). **E** Endogenous protein interaction (green dots) between MCL1 and mTOR or RICTOR was visualized by proximity ligation assays in A549, PC9 and NCI-H3122 cells treated with indicated inhibitors (trametinib: 1  $\mu$ M; erlotinib: 1  $\mu$ M; crizotinib: 3  $\mu$ M). Cell nuclei were stained with DAPI. Scale bar, 10  $\mu$ m. **F** A549, PC9 and NCI-H3122 cells were treated with indicated inhibitors over a time course (trametinib: 1  $\mu$ M; erlotinib: 1  $\mu$ M; crizotinib: 3  $\mu$ M). Endogenous MCL1 protein was immunoprecipitated and probed for RICTOR interaction. **G** Purified MCL1 protein was subjected to in vitro kinase assays with RICTOR immunoprecipitates. Indicated proteins were analyzed by immunoblotting. **H** A549, PC9 and NCI-H3122 cells were treated with indicated inhibitors (trametinib: 1  $\mu$ M; erlotinib: 1  $\mu$ M; crizotinib: 3  $\mu$ M; AZD8055: 1  $\mu$ M). Endogenous MCL1 protein was immunoprecipitated and analyzed by immunoblotting.

been well-documented to be regulated by mTORC1 via cap-dependent protein translation [44]. However, we found that adaptive MCL1 upregulation under initial targeted therapies turned out to be tuned by mTORC2 rather than mTORC1. Detailed dissection ruled out the role of canonical mTORC2 substrates, including AKT, PKC and SGK. Instead, we presented compelling evidence that mTORC2 bound and phosphorylated MCL1 at S64, leading to enhanced protein interaction between MCL1 and BIM. Of note, MCL1 harbors multiple phosphorylation sites catalyzed by GSK3 $\beta$ , CDK1, etc., which may display distinct functional impact on cell apoptosis [35]. In addition, although earlier work has implicated mTORC2 in mitochondrial physiology [45], the exact mechanisms for how mTORC2 is translocated onto mitochondria to complex with MCL1 remain to be elucidated.

For patients receiving targeted interventions, pathologic complete response is generally associated with long-term survival. When residual disease exists, the prognosis is typically worse [4, 5]. Thus, identifying novel regimens to maximize the initial therapeutic effects has substantial benefits as compared with salvage strategies upon cancer recurrence. Nevertheless, the ability to inhibit tumor adequately is often limited by safety issues, and numerous attempts to deploy combination therapies have been complicated by severe adverse reactions. Despite that a multitude of small-molecule inhibitors against PI3K, mTOR and MCL1 have entered clinical development [46–48], considering their crucial function in many vital normal cell types, the feasibility of continuous drug administration in addition to standard TKI treatment is conceivably dismal. Our findings of induced therapeutic susceptibility to MCL1 inhibition prompted us to design brief and upfront combinational protocols of concurrently targeting oncogenic driver and adaptive MCL1 preservation, in order to forestall the onset of drug tolerance while restraining potential systemic toxicity. Moreover, pharmacological perturbation at low or high doses exhibited comparable efficiency to evoke cell apoptosis and impede DTP formation, corroborating the recently described concept of vertical inhibition approach [49]. Finally, MCL1-mediated adaptation could be a general cell-protective mechanism in response to a wide spectrum of molecular targeted agents, and our study may have broader implications for the treatment of other oncogene-addicted human malignancies beyond NSCLC. The safety and efficacy of transient polytherapy should be evaluated in prospective clinical trials.

## MATERIALS AND METHODS

### Cell culture and reagents

The human lung cancer cell lines were purchased from the American Type Culture Collection (ATCC) or Japanese Collection of Research Bioresources Cell Bank (JCRB). All cell lines were routinely tested for mycoplasma contamination and cell identity. Cells were cultured in RPMI1640 (Life Technologies) supplemented with l-glutamine (2 mM), penicillin (100 U/

ml), streptomycin (100  $\mu$ g/ml), and 10% fetal bovine serum (Gibco). Small-molecule inhibitors were purchased from Selleck Chemicals and were reconstituted in DMSO (Sigma-Aldrich) at a stock concentration of 10 mM.

### Plasmids and sgRNA

The primers for mutagenesis and sgRNA sequences were provided in Supplementary Table 1. The MCL1 mutant constructs were generated using the Q5 Site-Directed Mutagenesis Kit (New England Biolabs) and verified by Sanger sequencing. CRISPR-Cas9 system was used to knock out indicated genes. For virus production, HEK293T cells in 10-cm dish were co-transfected with 5  $\mu$ g of lentiviral constructs, 5  $\mu$ g of plasmid delta 8.9, and 3  $\mu$ g of plasmid VSVG, and incubated at 37  $^{\circ}$ C. The medium was replaced after 12 hours. Virus-containing medium was collected 48 h after transfection and supplemented with 8 mg/mL polybrene to infect target cells in 6-well dishes. Infected cells were selected with 2 to 5  $\mu$ g/mL puromycin.

### Cell viability and apoptosis assays

Cell viability was determined by the CellTiter-Glo Assay Kit (Promega) according to the manufacturer's instructions. For visualization, cells were fixed with 4% paraformaldehyde and stained with 0.1% crystal violet. Cell apoptosis was detected by the Caspase-Glo 3/7 Assay Kit (Promega). To measure drug combination effects, cells were seeded into 96-well plates at a density of 3000–5000 cells per well. After 24 hours, cells were treated with increasing concentrations of two different inhibitors in a 7  $\times$  7 matrix. After incubation with inhibitors for 72 h, cell viability was determined using the CellTiter-Glo Assay Kit. The Bliss synergy scores were calculated by the equation  $(A + B) - A \times B$ . A or B was the fractional growth inhibition induced by the two inhibitors at a particular dose, respectively.

### Western blotting analysis

Cells were lysed in RIPA buffer (50 mM Tris pH 7.4, 150 mM NaCl, 1% NP-40, 0.1% SDS, 2  $\mu$ M EDTA) supplemented with protease inhibitors and phosphatase inhibitors (Roche). Protein concentrations were quantified using Pierce BCA Protein Assay Kit (Thermo Scientific). Equal amounts of proteins (15  $\mu$ g) were resolved by 10% SDS-PAGE and subjected to Western blot. The following primary antibodies were from Cell Signaling Technology: MCL1 (#39224), p-MCL1 (#13297), BCL2 (#2870), BCLXL (#2764), BCLW (#2724), BIM (#2933), PUMA (#4976), NOXA (#14766), BID (#2002), BAD (#9239), BAX (#5023), BAK (#6947), Cytochrome c (#4280), MULE (#5695), PARP (#9542), cleaved PARP (#5625), cleaved caspase-3 (#9664), p-ERK (#9101), ERK (#4695), p-AKT (#4060), AKT (#4691), p-mTOR (#2974), mTOR (#2983), p-RPS6 (#2211), p-NDRG1 (#5482),  $\alpha$ -tubulin (#2125), VDAC1 (#4661), GAPDH (#8884), H3 (#12648). Antibodies against GSDME (ab215191) and p-BAD (ab129192) were purchased from Abcam. Antibody against FBW7 (A301-720A) was purchased from Bethyl Laboratories. For subcellular fractionation assay, cells were fractionated with the Qproteome Cell Compartment Kit (Qiagen) and equivalent amounts of fractionated cell lysates were analyzed by immunoblotting.

Uncropped Western blots are provided in Supplementary Material.

### Immunoprecipitation assays

Cells were lysed on ice for 30 min in Pierce IP Lysis Buffer (25 mM Tris pH 7.4, 150 mM NaCl, 1% NP-40, 5% glycerol, 1 mM EDTA) supplemented with



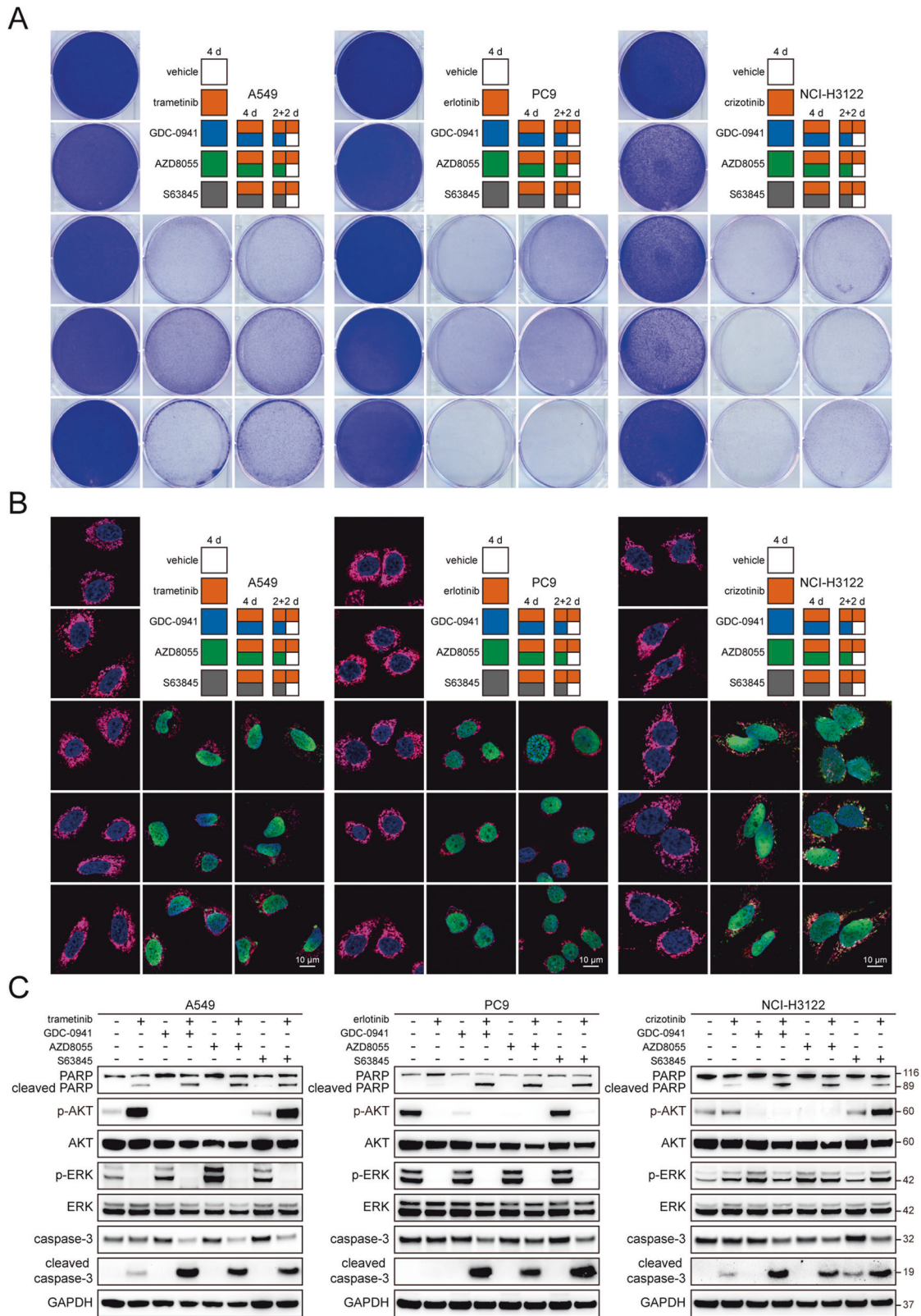


**Fig. 5** Transient targeting of adaptive MCL1 preservation provokes tumor cell death. **A** A549, PC9 and NCI-H3122 cells were treated with indicated inhibitors either alone or in combination as illustrated by the schematic diagram for 4 days (trametinib: 50 nM; erlotinib: 50 nM; crizotinib: 1  $\mu$ M; GDC-0941: 1  $\mu$ M; AZD8055: 0.5  $\mu$ M; S63845: 1  $\mu$ M). The remaining cells were analyzed by crystal violet staining. **B** A549, PC9 and NCI-H3122 cells were treated with indicated inhibitors either alone or in combination as illustrated by the schematic diagram for 4 days (trametinib: 50 nM; erlotinib: 50 nM; crizotinib: 1  $\mu$ M; GDC-0941: 1  $\mu$ M; AZD8055: 0.5  $\mu$ M; S63845: 1  $\mu$ M). Cells were stained for cytochrome c (pink), caspase-3/7 activatable nuclear dye (green) and nuclei (blue). Scale bar, 10  $\mu$ m. **C** A549, PC9 and NCI-H3122 cells were treated with indicated inhibitors for 48 h (trametinib: 50 nM; erlotinib: 50 nM; crizotinib: 1  $\mu$ M; GDC-0941: 1  $\mu$ M; AZD8055: 0.5  $\mu$ M; S63845: 1  $\mu$ M), and cell lysates were analyzed by immunoblotting. The following phosphorylation-specific antibodies were used: p-AKT (S473), p-ERK (T202/Y204).

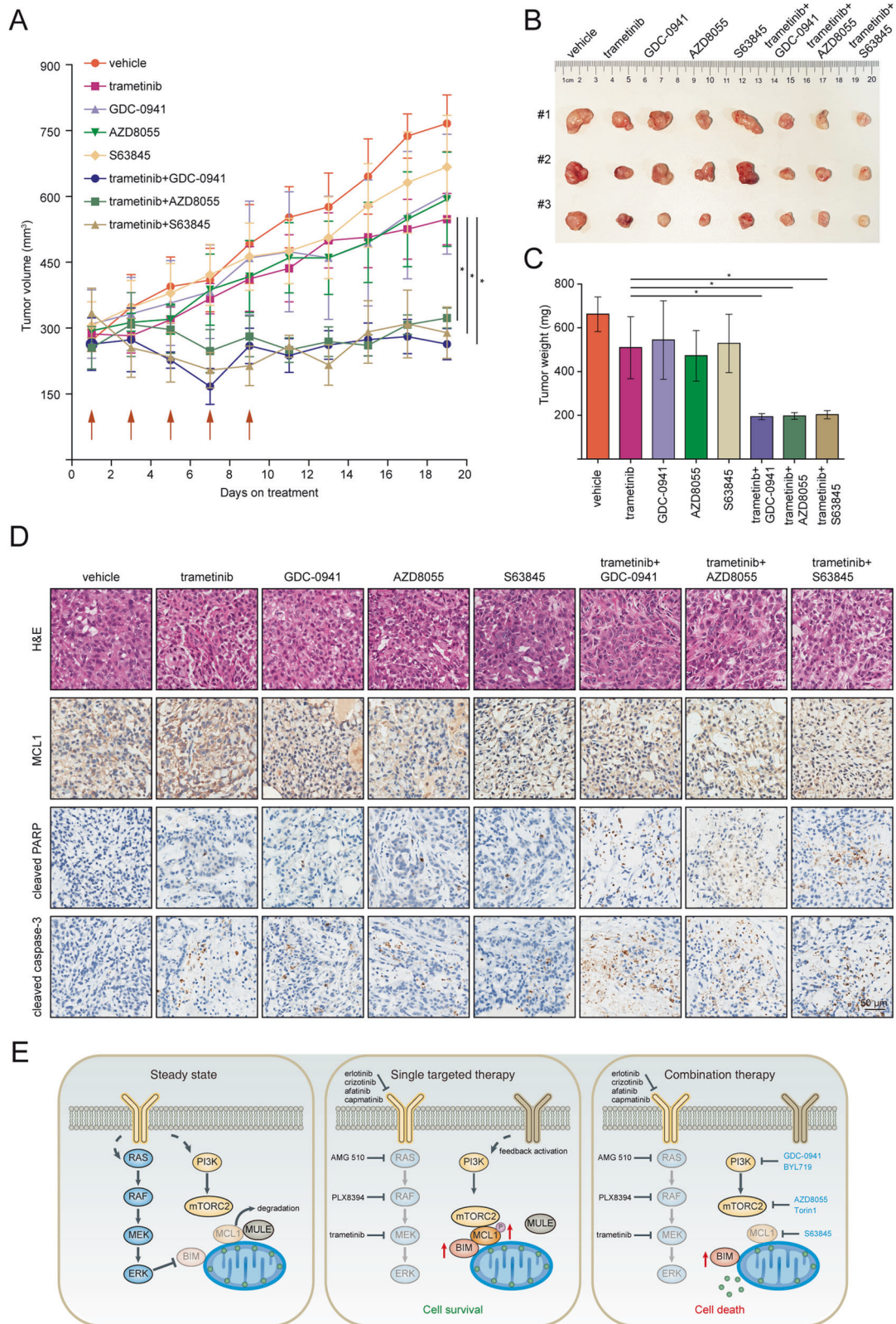


**Fig. 6** Transient targeting of adaptive MCL1 preservation may be exploited to augment therapeutic efficacy in vivo. **A** Tumor growth curves of A549 xenografts treated with vehicle control or indicated inhibitors. Each line represented the mean tumor volume and error bars indicated standard deviation (10 mice/group). Red arrows indicated combination treatments.  $*P < 0.05$ , ANOVA followed by Tukey's post-test. **B** Representative images of A549 xenografts treated with vehicle control or indicated inhibitors. **C** Quantification of A549 tumor weight in the vehicle control and inhibitor-treated groups.  $*P < 0.05$ , ANOVA followed by Tukey's post-test. **D** Representative images of H&E and immunohistochemistry staining for MCL1, cleaved PARP or cleaved caspase-3 in A549 tumor slices. Scale bar, 50  $\mu\text{m}$ . **E** A schematic model depicting the proposed role of adaptive MCL1 preservation in promoting tumor cell survival from molecular targeted therapies. Rational combination treatments provoke cell death and prevent DTP formation.



protease inhibitors. The lysates were centrifuged, and protein concentrations were determined by Pierce BCA Protein Assay Kit (Thermo Scientific). Equal amounts of cell lysates were immunoprecipitated with MCL1 antibody (ab32087, Abcam) and protein G agarose beads (E3403, Sigma-Aldrich) at 4 °C overnight. Beads were washed five times with IP lysis buffer and boiled for 10 min in Laemmli loading buffer. The immunoprecipitates and whole cell lysates were analyzed by immunoblotting.

### In vitro kinase assays

Immunoprecipitation of the mTORC2 complex and in vitro kinase assays were performed as previously described with slight modifications [50]. Cells were harvested and lysed in CHAPS lysis buffer (40 mM HEPES pH 7.5, 120 mM NaCl, 0.3% CHAPS, 1 mM EDTA, 10 mM glycerophosphate, 50 mM NaF, 10 mM pyrophosphate, 0.5 mM orthovanadate, and EDTA-free protease inhibitors). Cell lysates were centrifuged at 13,000 g for 10 min at 4 °C. The supernatant was immunoprecipitated with 4 µg of anti-RICTOR antibodies by incubation with rotation for 2 hours at 4 °C, followed by addition of 25 µL protein G beads (Sigma-Aldrich) and incubation for an additional hour. Then the protein G beads were washed 3 times with CHAPS lysis buffer and twice with kinase buffer (25 mM HEPES pH 7.5, 100 mM potassium acetate, 2 mM MgCl<sub>2</sub>). Immunoprecipitates were incubated for 30 min at 37 °C in a final volume of 30 µL kinase buffer containing 250 ng of MCL1 protein (ProSpec, PRO-1202) and 500 µM ATP. The reaction was terminated by adding SDS sample buffer and samples were subjected to electrophoresis and immunoblotting.

### Immunofluorescence microscopy

Cells cultured in a confocal chamber (Ibidi) were fixed with 4% paraformaldehyde for 15 min at room temperature (RT) and permeabilized with 0.5% Triton X-100 for 10 min. Cells were blocked with 5% BSA in PBS for 30 min before incubating with primary antibodies for 2 hours at RT, followed by labeling with fluorescein-conjugated secondary antibodies for 1 hour and DAPI counterstaining for 5 min in the dark. The staining was observed using a confocal laser scanning microscopy (Leica). Caspase-3/7 activity was assessed by CellEvent Caspase-3/7 Green Detection Reagent (C10423, Thermo Scientific). Mitochondria were labeled with MitoTracker Red probes (M7512, Thermo Scientific) according to the manufacturer's protocol.

### Proximity ligation assays

In situ proximity ligation assay (PLA) was performed using the Duolink Detection Kit (Sigma-Aldrich) according to the manufacturer's instructions. Briefly, cells were fixed in 4% paraformaldehyde for 15 min, permeabilized with 0.1% Triton X-100 for 10 min, and blocked with blocking solution for 60 min at 37 °C. Cells were incubated with primary antibodies against MCL1 (#39224, Cell Signaling Technology) and RICTOR (PLA0309, Sigma-Aldrich), or MCL1 (GTx84135, GeneTex) and mTOR (PLA0114, Sigma-Aldrich) at 4 °C overnight. Cells were then incubated with anti-mouse PLUS and anti-rabbit MINUS oligonucleotide-conjugated secondary antibodies (PLA probes) for 1 h at 37 °C. Enzymatic ligation was performed at 37 °C for 30 min followed by PLA signal amplification at 37 °C for 100 min to allow the generation of a fluorescent signal (PLA signal) at sites where two oligonucleotide probes were in close proximity.

### Immunohistochemical staining

Human tissue samples were obtained in accordance with ethical guidelines of U.S. Common Rule. The study was approved by the Ethics Committee of Ren Ji Hospital and all patients signed informed consent. Formalin-fixed and paraffin-embedded samples were obtained after pathologic examination. The tissue sections were baked, dewaxed with xylene, passed through graded alcohols, and antigen retrieved with 10 mM citric sodium (pH 6.0) for 20 min in a steam pressure cooker. The slides were treated for 10 min with 3% H<sub>2</sub>O<sub>2</sub> in methanol to quench endogenous peroxidase activity, blocked with goat serum and incubated with primary antibody against MCL1 (#39224, Cell Signaling Technology) at 4 °C overnight. Slides were then subjected to incubation with horseradish peroxidase-conjugated secondary antibody for 1 h at RT. Antigen visualization was performed using 3,3'-diaminobenzidine (DAB) chromogen (Vector Laboratories). Slides were counterstained with hematoxylin, dehydrated and cover slipped with mounting solution (Invitrogen).

### In vivo studies

Tumor cells (1 × 10<sup>6</sup>) were mixed with Matrigel (BD Biosciences) and injected subcutaneously into the dorsal flank of female BALB/c Nude mice

(5 weeks of age). Once the mean tumor volume reached 200–300 mm<sup>3</sup>, mice were randomized into vehicle and treatment groups (10 mice each). For long-term treatment, trametinib was given at a dose of 0.5 mg/kg/day via gavage, erlotinib was given at a dose of 5 mg/kg every other day via gavage, and crizotinib was given at a dose of 60 mg/kg/day via gavage. For transient combination treatment, trametinib was given at a dose of 0.5 mg/kg/day via gavage, GDC-0941 was given at a dose of 100 mg/kg/day via gavage for five days, AZD8055 was given at a dose of 20 mg/kg/day via gavage for five days, and S63845 was given at a dose of 25 mg/kg/day via tail vein injection for five days. Tumor volumes were measured with a caliper and calculated as length × width<sup>2</sup> × 0.52. At the end of the study, mice were sacrificed, and the xenografts were harvested and imaged. For all experiments, animals were randomly chosen, and no statistical method was used to determine sample sizes. The institutional animal care and use committee of Ren Ji Hospital approved animal protocols and all experiments were performed in accordance with Ren Ji Hospital policies on the care, welfare, and treatment of laboratory animals.

### RNA sequencing and analysis

Total RNA was extracted using RNeasy Plus Mini Kit (Qiagen) according to the manufacturer's instructions and qualified by RNA Nano 6000 Assay Kit of the Bioanalyzer 2100 system. Sequencing libraries were prepared using the NEBNext Ultra RNA Library Prep Kit for Illumina (NEB). Clustering of the index-coded libraries on a cBot Cluster Generation System using TruSeq PE Cluster Kit v3-cBot-HS (Illumina), and the library preparations were sequenced on an Illumina Novaseq platform to generate 30 million 150 bp paired-end reads (Novogene, Beijing). Analyses were based on clean data which were obtained by removing low-quality reads and reads containing adapters or ploy-N sequences. The index of the reference genome was built using Bowtie, and clean reads were aligned to the reference genome using Hisat2. FeatureCounts was used to count the reads mapped to each gene. Differential expression analysis was performed using the edgeR package. P-values were adjusted using the Benjamini-Hochberg procedure for controlling the false discovery rate. Genes with an adjusted P-value of < 0.05 were considered differentially expressed. The results were validated using quantitative PCR analysis.

### Statistical analysis

Statistical analysis was performed with GraphPad Prism version 7. The researchers involved in this study were not blinded during sample collection or data analysis. Sample sizes were selected based on preliminary results to ensure a power of 80% with 95% confidence. Statistical analyses were justified to meet the assumptions such as similar variances and normal distribution. No data points were excluded. In all experiments, comparisons between two groups were based on two-sided Student's *t*-test, and one-way analysis of variance (ANOVA) was used to test for differences among more groups. P-values of < 0.05 were considered statistically significant.

### DATA AVAILABILITY

All original data are available upon request from the authors.

### REFERENCES

1. Thai AA, Solomon BJ, Sequist LV, Gainor JF, Heist RS. Lung cancer. *Lancet* 2021;398:535–54.
2. Herbst RS, Morgensztern D, Boshoff C. The biology and management of non-small cell lung cancer. *Nature* 2018;553:446–54.
3. Blatter S, Rottenberg S. Minimal residual disease in cancer therapy—Small things make all the difference. *Drug Resist Update*. 2015;21:221–10.
4. Bivona TG, Doebele RC. A framework for understanding and targeting residual disease in oncogene-driven solid cancers. *Nat Med*. 2016;22:472–8.
5. Luskin MR, Murakami MA, Manalis SR, Weinstock DM. Targeting minimal residual disease: a path to cure? *Nat Rev Cancer*. 2018;18:255–63.
6. Sharma SV, Lee DY, Li B, Quinlan MP, Takahashi F, Maheswaran S, et al. A chromatin-mediated reversible drug-tolerant state in cancer cell subpopulations. *Cell* 2010;141:69–80.
7. Ramirez M, Rajaram S, Steininger RJ, Osipchuk D, Roth MA, Morinishi LS, et al. Diverse drug-resistance mechanisms can emerge from drug-tolerant cancer persister cells. *Nat Commun*. 2016;7:10690.
8. Hata AN, Niederst MJ, Archibald HL, Gomez-Caraballo M, Siddiqui FM, Mulvey HE, et al. Tumor cells can follow distinct evolutionary paths to become resistant to epidermal growth factor receptor inhibition. *Nat Med*. 2016;22:262–9.



9. Rehman SK, Haynes J, Collignon E, Brown KR, Wang Y, Nixon AML, et al. Colorectal Cancer Cells Enter a Diapause-like DTP State to Survive Chemotherapy. *Cell* 2021;184:226–42.
10. Chandralapaty S. Negative feedback and adaptive resistance to the targeted therapy of cancer. *Cancer Disco*. 2012;2:311–9.
11. Rosell R, Karachaliou N, Morales-Espinosa D, Costa C, Molina MA, Sansano I, et al. Adaptive resistance to targeted therapies in cancer. *Transl Lung Cancer Res*. 2013;2:152–9.
12. Pazarentzos E, Bivona TG. Adaptive stress signaling in targeted cancer therapy resistance. *Oncogene* 2015;34:5599–606.
13. Marine JC, Dawson SJ, Dawson MA. Non-genetic mechanisms of therapeutic resistance in cancer. *Nat Rev Cancer*. 2020;20:743–56.
14. Guler GD, Tindell CA, Pitti R, Wilson C, Nichols K, KaiWai Cheung T, et al. Repression of Stress-Induced LINE-1 expression protects cancer cell subpopulations from lethal drug exposure. *Cancer Cell*. 2017;32:221–37.
15. Liao BB, Sievers C, Donohue LK, Gillespie SM, Flavahan WA, Miller TE, et al. Adaptive chromatin remodeling drives glioblastoma stem cell plasticity and drug tolerance. *Cell Stem Cell*. 2017;20:233–46.e7
16. Lito P, Pratilas CA, Joseph EW, Tadi M, Halilovic E, Zubrowski M, et al. Relief of profound feedback inhibition of mitogenic signaling by RAF inhibitors attenuates their activity in BRAFV600E melanomas. *Cancer Cell*. 2012;22:668–82.
17. Lito P, Rosen N, Solit DB. Tumor adaptation and resistance to RAF inhibitors. *Nat Med*. 2013;19:1401–9.
18. Lee HJ, Zhuang G, Cao Y, Du P, Kim HJ, Settleman J. Drug resistance via feedback activation of Stat3 in oncogene-addicted cancer cells. *Cancer Cell*. 2014;26:207–21.
19. Rusan M, Li K, Li Y, Christensen CL, Abraham BJ, Kwiatkowski N, et al. Suppression of Adaptive Responses to Targeted Cancer Therapy by Transcriptional Repression. *Cancer Disco*. 2018;8:59–73.
20. Costa DB, Halmos B, Kumar A, Schumer ST, Huberman MS, Boggon TJ, et al. BIM mediates EGFR tyrosine kinase inhibitor-induced apoptosis in lung cancers with oncogenic EGFR mutations. *PLoS Med*. 2007;4:1669–79.
21. Ng KP, Hillmer AM, Chuah CT, Juan WC, Ko TK, Teo AS, et al. A common BIM deletion polymorphism mediates intrinsic resistance and inferior responses to tyrosine kinase inhibitors in cancer. *Nat Med*. 2012;18:521–8.
22. Singh R, Letai A, Sarosiek K. Regulation of apoptosis in health and disease: the balancing act of BCL-2 family proteins. *Nat Rev Mol Cell Biol*. 2019;20:175–93.
23. Kotschy A, Szlavik Z, Murray J, Davidson J, Maragno AL, Le Toumelin-Braizat G, et al. The MCL1 inhibitor S63845 is tolerable and effective in diverse cancer models. *Nature* 2016;538:477–82.
24. Zhong Q, Gao W, Du F, Wang X. Mule/ARF-BP1, a BH3-only E3 ubiquitin ligase, catalyzes the polyubiquitination of Mcl-1 and regulates apoptosis. *Cell* 2005;121:1085–95.
25. Inuzuka H, Shaik S, Onoyama I, Gao D, Tseng A, Maser RS, et al. SCF(FBW7) regulates cellular apoptosis by targeting MCL1 for ubiquitylation and destruction. *Nature* 2011;471:104–9.
26. Wertz IE, Kusam S, Lam C, Okamoto T, Sandoval W, Anderson DJ, et al. Sensitivity to antitubulin chemotherapeutics is regulated by MCL1 and FBW7. *Nature* 2011;471:110–4.
27. Chen R, Keating MJ, Gandhi V, Plunkett W. Transcription inhibition by flavopiridol: Mechanism of chronic lymphocytic leukemia cell death. *Blood* 2005;106:2513–9.
28. Liu GY, Sabatini DM. mTOR at the nexus of nutrition, growth, ageing and disease. *Nat Rev Mol Cell Biol*. 2020;21:183–203.
29. Kobayashi S, Lee SH, Meng XW, Mott JL, Bronk SF, Werneburg NW, et al. Serine 64 phosphorylation enhances the antiapoptotic function of Mcl-1. *J Biol Chem*. 2007;282:18407–17.
30. Boshuizen J, Peeper DS. Rational cancer treatment combinations: An urgent clinical need. *Mol Cell*. 2020;78:1002–18.
31. Nangia V, Siddiqui FM, Caenepeel S, Timonina D, Bilton SJ, Phan N, et al. Exploiting MCL1 Dependency with Combination MEK + MCL1 Inhibitors Leads to Induction of Apoptosis and Tumor Regression in KRAS-Mutant Non-Small Cell Lung Cancer. *Cancer Disco*. 2018;8:1598–613.
32. Montero J, Gstalder C, Kim DJ, Sadowicz D, Miles W, Manos M, et al. Destabilization of NOXA mRNA as a common resistance mechanism to targeted therapies. *Nat Commun*. 2019;10:5157.
33. Sale MJ, Minihane E, Monks NR, Gilley R, Richards FM, Schifferli KP, et al. Targeting melanoma's MCL1 bias unleashes the apoptotic potential of BRAF and ERK1/2 pathway inhibitors. *Nat Commun*. 2019;10:5167.
34. Munkhbaatar E, Dietzen M, Agrawal D, Anton M, Jesinghaus M, Boxberg M, et al. MCL-1 gains occur with high frequency in lung adenocarcinoma and can be targeted therapeutically. *Nat Commun*. 2020;11:4527.
35. Senichkin VV, Streletskaia AY, Gorbunova AS, Zhivotovsky B, Kopeina GS. Saga of Mcl-1: regulation from transcription to degradation. *Cell death Differ*. 2020;27:405–19.
36. Senichkin VV, Streletskaia AY, Zhivotovsky B, Kopeina GS. Molecular Comprehension of Mcl-1: From Gene Structure to Cancer Therapy. *Trends Cell Biol*. 2019;29:549–62.
37. Yecies D, Carlson NE, Deng J, Letai A. Acquired resistance to ABT-737 in lymphoma cells that up-regulate MCL-1 and BFL-1. *Blood* 2010;115:3304–13.
38. Campbell KJ, Bath ML, Turner ML, Vandenberg CJ, Bouillet P, Metcalf D, et al. Elevated Mcl-1 perturbs lymphopoiesis, promotes transformation of hematopoietic stem/progenitor cells, and enhances drug resistance. *Blood* 2010;116:3197–207.
39. He L, Torres-Lockhart K, Forster N, Ramakrishnan S, Greninger P, Garnett MJ, et al. Mcl-1 and FBW7 control a dominant survival pathway underlying HDAC and Bcl-2 inhibitor synergy in squamous cell carcinoma. *Cancer Disco*. 2013;3:324–37.
40. Wu X, Luo Q, Zhao P, Chang W, Wang Y, Shu T, et al. MGMT-activated DUB3 stabilizes MCL1 and drives chemoresistance in ovarian cancer. *Proc Natl Acad Sci USA*. 2019;116:2961–6.
41. Song KA, Hosono Y, Turner C, Jacob S, Lochmann TL, Murakami Y, et al. Increased Synthesis of MCL-1 Protein Underlies Initial Survival of EGFR-Mutant Lung Cancer to EGFR Inhibitors and Provides a Novel Drug Target. *Clin Cancer Res*. 2018;24:5658–72.
42. Wullemme-Toumi S, Trichet V, Gomez-Bougie P, Gratas C, Bataille R, Amiot M. Reciprocal protection of Mcl-1 and Bim from ubiquitin-proteasome degradation. *Biochem Biophys Res Commun*. 2007;361:865–9.
43. Warr MR, Acoca S, Liu Z, Germain M, Watson M, Blanchette M, et al. BH3-ligand regulates access of MCL-1 to its E3 ligase. *FEBS Lett*. 2005;579:5603–8.
44. Hsieh AC, Costa M, Zollo O, Davis C, Feldman ME, Testa JR, et al. Genetic dissection of the oncogenic mTOR pathway reveals druggable addiction to translational control via 4EBP-eIF4E. *Cancer Cell*. 2010;17:249–61.
45. Betz C, Stracka D, Prescianotto-Baschong C, Frieden M, Demaurex N, Hall MN. Feature Article: mTOR complex 2-Akt signaling at mitochondria-associated endoplasmic reticulum membranes (MAM) regulates mitochondrial physiology. *Proc Natl Acad Sci USA*. 2013;110:12526–34.
46. Janku F, Yap TA, Meric-Bernstam F. Targeting the PI3K pathway in cancer: are we making headway? *Nat Rev Clin Oncol*. 2018;15:273–91.
47. Tron AE, Belmonte MA, Adam A, Aquila BM, Boise LH, Chiarparin E, et al. Discovery of Mcl-1-specific inhibitor AZD5991 and preclinical activity in multiple myeloma and acute myeloid leukemia. *Nat Commun*. 2018;9:5341.
48. Caenepeel S, Brown SP, Belmontes B, Moody G, Keegan KS, Chui D, et al. AMG 176, a Selective MCL1 Inhibitor, Is Effective in Hematologic Cancer Models Alone and in Combination with Established Therapies. *Cancer Disco*. 2018;8:1582–97.
49. Ryan MB, Fece de la Cruz F, Phat S, Myers DT, Wong E, Shahzade HA, et al. Vertical Pathway Inhibition Overcomes Adaptive Feedback Resistance to KRAS(G12C) Inhibition. *Clin Cancer Res*. 2020;26:1633–43.
50. Sarbassov DD, Guertin DA, Ali SM, Sabatini DM. Phosphorylation and regulation of Akt/PKB by the rictor-mTOR complex. *Science* 2005;307:1098–101.

## ACKNOWLEDGEMENTS

We acknowledge all lab members for technical support and helpful discussions. This work was supported by the National Natural Science Foundation of China (81922047 and 82172596 to GZ; 82072560 to XZ), Shanghai Municipal Education Commission-Gaofeng Clinical Medicine Grant Support (20161313 to GZ), Shanghai Collaborative Innovation Center for Translational Medicine (TM202005 to GZ), and innovative research team of high-level local universities in Shanghai (SHSMU-ZLXC20210200 to GZ).

## AUTHOR CONTRIBUTIONS

GZ, JT, ZY, and XZ conceptualized the study. KS, HL, ZZ, YF, JW, SZ, PM, KY, SZ, HS and WS conducted the experiments and analyzed the data. KS and M-CC performed the bioinformatics analyses. GZ and KS wrote the manuscript. All the authors read and approved the manuscript.

## COMPETING INTERESTS

The authors declare no competing interests.

## ETHICS APPROVAL

The institutional animal care and use committee of Ren Ji Hospital approved animal protocols. The study using human tissues was approved by the Ethics Committee of Ren Ji Hospital and all patients signed informed consent.

**ADDITIONAL INFORMATION**

**Supplementary information** The online version contains supplementary material available at <https://doi.org/10.1038/s41418-022-01064-2>.

**Correspondence** and requests for materials should be addressed to Xiaojing Zhao, Zhuang Yu, Jian Tang or Guanglei Zhuang.

**Reprints and permission information** is available at <http://www.nature.com/reprints>

**Publisher's note** Springer Nature remains neutral with regard to jurisdictional claims in published maps and institutional affiliations.

Springer Nature or its licensor holds exclusive rights to this article under a publishing agreement with the author(s) or other rightsholder(s); author self-archiving of the accepted manuscript version of this article is solely governed by the terms of such publishing agreement and applicable law.